

UNIVERSITY OF HELSINKI

REPORT SERIES IN PHYSICS

HU-P-D84

# Phenomenological model for electronic stopping of low-velocity ions in crystalline solids

**Jussi Sillanpää**

Accelerator Laboratory  
Department of Physics  
Faculty of Science  
University of Helsinki  
Helsinki, Finland

*ACADEMIC DISSERTATION*

*To be presented, with the permission of the Faculty of Science of the University of Helsinki, for public criticism in Auditorium I of the Department of Physics, on May 15th, 2000, at 12 o'clock noon.*

Saarijärvi 2000

---

ISBN 951-45-9371-5 (printed version)  
ISSN 0356-0961  
Saarijärvi 2000  
Gummeruksen kirjapaino

ISBN 951-45-9179-8 (PDF version)  
Helsinki 2000  
Helsingin yliopiston verkkojulkaisut

J. Sillanpää: Phenomenological model for electronic stopping of low-velocity ions in crystalline solids, University of Helsinki, 2000, 39 p.+appendices, University of Helsinki Report Series in Physics, HU-P-D84, ISSN 0356-0961, ISBN 951-45-9371-5

Classification (INSPEC): A3410

Keywords: Electronic stopping, molecular dynamics, ion implantation, ion beam mixing, silicon

## **ABSTRACT**

Understanding the slowing down process of ions in solids is not only an interesting problem of theoretical physics but fundamentally important to many analysis and manufacturing methods as well. A particularly acute problem is the accurate prediction of electronic slowing down in crystalline materials. The purpose of the work described in this thesis is to study, measure and model the energy loss mechanisms, particularly electronic stopping.

A local electronic stopping model for low-energy ions has been developed and used in molecular dynamics (MD) computer simulations. The model has been tested and its results compared with other models and experiments. Our model achieved good accuracy. Ways to develop the model further are discussed.

Comparison of experimental and simulated range profiles has been used to determine the electronic stopping of He in several metals relevant to fusion research. Correction factors for the commonly used ZBL stopping were obtained.

Finally, MD simulations have been used to study ion beam mixing in silicon. The results of our simulations have been compared with experiments and the merits of using mixing experiments to develop better interatomic potentials have been considered.

## Contents

<b>ABSTRACT</b>	<b>1</b>
<b>1 INTRODUCTION</b>	<b>3</b>
<b>2 STRUCTURE AND PURPOSE OF THIS STUDY</b>	<b>3</b>
<b>3 EFFECTS OF ION BEAMS ON MATERIALS</b>	<b>6</b>
<b>4 EXPERIMENTAL TECHNIQUES FOR MEASURING STOPPING AND RANGES</b>	<b>10</b>
4.1 ELECTRONIC STOPPING . . . . .	10
4.2 RANGES . . . . .	12
<b>5 PRINCIPLES OF RANGE CALCULATIONS</b>	<b>14</b>
<b>6 GENERALLY USED ELECTRONIC STOPPING PARAMETRIZATIONS</b>	<b>18</b>
<b>7 RANGE CALCULATIONS AND STUDIES OF STOPPING POWERS</b>	<b>22</b>
7.1 CORRECTION FACTORS FOR THE ZBL STOPPING POWERS . . . . .	22
7.2 ION BEAM MIXING AND INTERATOMIC POTENTIALS . . . . .	23
7.3 A LOCAL ELECTRONIC STOPPING MODEL BASED ON THE BK THEORY . . . . .	23
<b>8 CONCLUSIONS</b>	<b>29</b>
<b>ACKNOWLEDGEMENTS</b>	<b>30</b>
<b>REFERENCES</b>	<b>31</b>

## 1 INTRODUCTION

Ion beams are used to analyze materials [1] and to modify their mechanical, optical and electrical properties [2]. In order to use ion beam methods, we need to understand the interactions between energetic ions and materials, especially the forces that slow down the ions [3]. Accurate modelling of electronic stopping is a particularly pertinent problem [4].

Computer simulations have long been an integral part of ion beam physics. By using computer simulations based on molecular dynamics (MD) [5], we can study the interactions between ions and matter. Range calculations, where the depth distributions of dopants are calculated, are particularly important to the semiconductor industry [6]. As the size of semiconductor components decreases, the implantation energies must decrease as well and the importance of accurate computer simulations is further increased [6–9]. Decreasing implantation energies dictate a reduced thermal budget which will result in a decrease in the amount of post-implant diffusion, which increases the value of accurate range calculations to industry. Ions moving in crystal channels, where the electron and atom densities are significantly below average, present quite a difficult challenge to simulation programs [10]. The calculation of accurate range profiles in such circumstances demands a local electronic stopping parametrization [11].

Several local electronic stopping models for low velocity ions have been proposed during the last decade. Unfortunately, the models have been either designed only for one ion-target combination or one material, or contained one or more free parameters. A transferable, accurate and physically well-motivated model has not been formulated. The model described in this thesis aims to fulfill these requirements. It is based on a three-dimensional electron distribution, contains no free parameters and can therefore be used to calculate the stopping of any ion in any target without a parameter fitting process. The model has been tested for stopping in silicon. It was found that the accuracy of the model, with the exception of the  $\langle 110 \rangle$  channel, is good.

## 2 STRUCTURE AND PURPOSE OF THIS STUDY

This study consists of the following four articles published or accepted to be published in refereed international scientific journals.

### Summaries of the original papers

**Paper I: Stopping of 5-100 keV helium in molybdenum, chromium, copper and nickel**, J. Sillanpää, E. Vainonen-Ahlgren, P. Haussalo, and J. Keinonen, *Nucl. Instr. Meth. Phys. Res. B* **142**, 1 (1998).

We determine the stopping powers for 5 – 100 keV helium in molybdenum, chromium, copper and nickel by comparing experimental range profiles with simulated ones. We obtain correction factors for the commonly used electronic stopping powers calculated using the formulation of J.F. Ziegler, J. Biersack and U. Littmark.

**Paper II: Heat spike and ballistic contributions to mixing in Si**, J. Tarus, K. Nordlund, J. Sillanpää, and J. Keinonen, *Nucl. Instr. Meth. Phys. Res. B* **153**, 378 (1999).

We study atomic mixing in silicon with the molecular dynamics (MD) method. We present a method for calculating the mixing produced by high-energy beams with MD simulations and compare the results with experiments. Good agreement with experimental results is obtained. The ballistic collisions are shown to be more important to mixing than the heat spike.

**Paper III: Channeling in Manufacturing Sharp Junctions: a Molecular Dynamics Study**, J. Sillanpää, K. Nordlund, and J. Keinonen, *Physica Scripta* **T79**, 272 (1999).

The shape of range profiles of commonly used dopants implanted into silicon are studied with MD simulations. We compare our simulations with experiments and present results for the sharpness of the as-implanted range profiles.

**Paper IV: Electronic stopping of Silicon from a 3D charge distribution**, J. Sillanpää, K. Nordlund, and J. Keinonen, *accepted for publication in Phys. Rev. B*.

We present and test a local electronic stopping model for low energy ions, based on the Brand-Kitagawa theory and incorporating a version of the Firsov model. The model treats the charge density of the target accurately with a three-dimensional electron distribution. We obtain good accuracy, except in the  $\langle 110 \rangle$  direction. Preliminary results, obtained from an earlier version of the model, were published by J. Sillanpää in *Nucl. Instr. Meth. Phys. Res. B* **164-165**, 302 (2000).

The purpose of this study was to improve our knowledge of low energy stopping powers, particularly to develop an electronic stopping parametrization for low-velocity ions that can be used in all crystal directions.

In the first article the electronic stopping of helium ions in several metals relevant to fusion research is determined. In paper II, we study ion-beam induced mixing in silicon. It is found that most of the mixing is caused by the primary recoils and therefore the mixing experiments studied do not yield much information on the quality of the equilibrium interatomic potential used. However, they do provide a test of the repulsive part of the potential and hence of the nuclear stopping.

In papers III and IV we study and test electronic stopping models. A local electronic stopping model for low energy ions is developed. The model can be used to predict the electronic slowing down in crystal channels as well as in non-channeling directions. Our model is based on the Brandt-Kitagawa (BK) theory, calculates the stopping from a three-dimensional charge distribution and has no free parameters. Article IV deals with the final version of the model and its capabilities. We find that, with the exception of the  $\langle 110 \rangle$  channel, the accuracy is good and discuss ways to further improve it.

All the publications above are the result of group work. All the range calculations in papers I, III and IV and most of those in paper II were performed by the author, who also participated in the writing of papers I and II and wrote most of papers III and IV. The stopping model presented in paper IV was fully developed by the author.

### 3 EFFECTS OF ION BEAMS ON MATERIALS

When energetic ions enter a material, they start to lose their kinetic energy and eventually stop. The particles experience a slowing force which is called the stopping power,

$$S = \frac{-dE}{dx}. \quad (1)$$

We can also define a quantity called the stopping cross section,

$$\sigma_s = \frac{-dE/dx}{N}, \quad (2)$$

where  $N$  is the atomic density of the material. The stopping cross section measures the contribution of a single atom to the stopping power of the material.

The kinetic energy of the ions is mainly transferred to heat, while some of it goes to creating damage in the material or detaching atoms from it (sputtering). At very high energies nuclear reactions and *bremsstrahlung* are also important. In the context of this thesis, however, they can be ignored [12].

Stopping is conventionally divided into two parts, namely the nuclear and electronic stopping,

$$S = S_n + S_e. \quad (3)$$

Nuclear stopping means the transfer of energy to target atoms via interatomic collisions. It is the dominant mode of energy transfer at low velocities (see Fig. 1). The ion can lose most of its energy in a single collision and its direction can change considerably. On the other hand, when the ion interacts with the electrons in the target material (electronic stopping), the energy transferred in one collision is small and the change in direction is negligible. Energetic ions incident on targets have four principal effects:

#### 1. Damage creation

The ions destroy the lattice structure of the target material, mostly because of nuclear stopping.

#### 2. Mixing

The energy given by the ions to the target atoms results in strong atom relocation modifying e.g. regular bi-layered structures, because of nuclear stopping.

#### 3. Sputtering

The ions detach atoms from the target, usually because of nuclear stopping.

#### 4. Doping

If the target is thick enough, the ions stop inside it and modify e.g. its electrical properties.



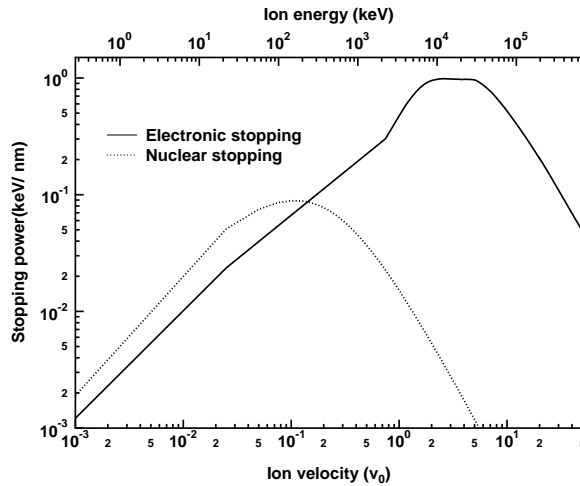


Figure 1: Stopping of  $^{11}\text{B}$  in silicon calculated using the ZBL parametrization [13] ( $v_0$  signifies the Bohr velocity).

In order to describe these phenomena and take advantage of them we must have a good understanding of stopping. Instead of stopping, the terms energy loss and slowing down are also used. Sometimes the nuclear stopping is referred to as elastic energy loss and the electronic stopping as inelastic energy loss. At the energies considered in this thesis, the nuclear stopping accounts for almost all damage and sputtering [2].

In a crystalline material the atoms form a periodic lattice. Consequently stopping is not constant because the structure has lattice directions, called channels, where atomic and electron densities are considerably lower than elsewhere in the crystal, see Figs. 2 and 3. Channeling means that ions entering a channel have considerably longer ranges than ions entering the crystal in non-channeling directions [14, 15]. Channeling is the result of not only a lower stopping in the center of the channel but also a focusing effect by the atoms at the edges of the channels. The effect was first seen in computer simulations [16] before it was verified with experimental range measurements [17].

Channeling is a significant phenomenon for implant energies from a keV up to several tens of MeV. High energy channeling is dominated by planar channeling (ions moving between sheets of atoms) whereas low energy channeling, of which we are interested, is dominated by axial channeling (ions moving between rows of atoms, see Fig. 3). The critical angle of channeling  $\theta_c$  is defined as the maximum angle of incidence of implanted ions to a channel between rows of atoms (axial channeling) or planes of atoms (planar channeling) so that the ion remains in a channeled trajectory. Starting from a two-dimensional analytical model [14, 21] it can be shown that the critical angle is inversely

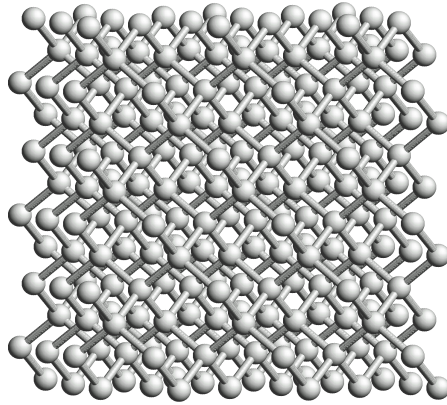


Figure 2: Diamond lattice of silicon seen from a non-channeling direction.

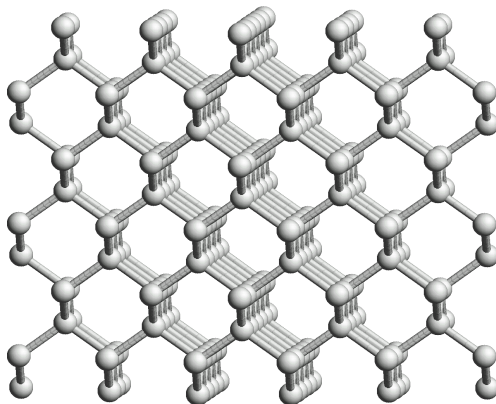


Figure 3:  $\langle 110 \rangle$  channels of the silicon lattice.

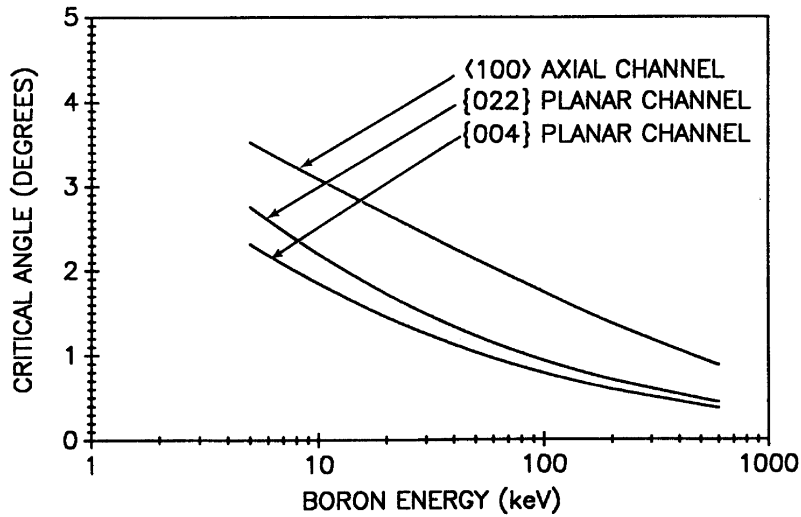


Figure 4: Critical channeling angles of boron in silicon [18].

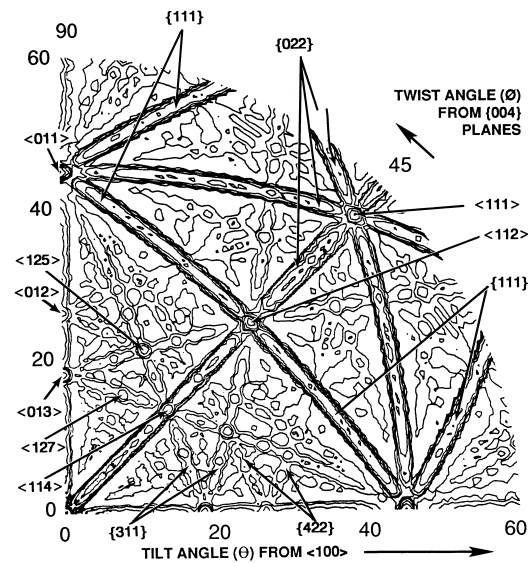


Figure 5: Channeling plot of the ranges of 100 keV boron in silicon [19]. The data is from computer simulations. The planar channels have elongated shapes, the axial channels appear as points. The contours are at 15, 30, 60, 120, 240 and 480 nm.

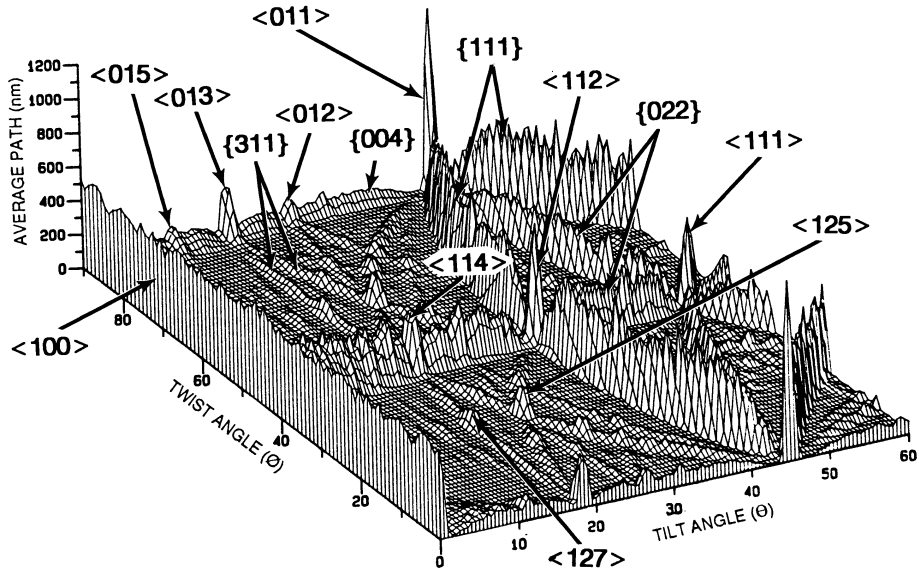


Figure 6: Perspective plot of the path lengths of 100 keV boron in silicon [19, 20]. The data is from computer simulations. The  $\langle 100 \rangle$  channel appears as a ridge on the left.

proportional to the square root of the implantation energy, see Fig. 4. This means that the importance of channeling increases as the implantation energies used in the semiconductor industry get lower and lower [6, 10, 22]. Channeling can be illustrated by backscattering or channeling maps obtained from experiments or computer simulations, such as the one in Fig. 5. Perspective plots, such as the one in Fig. 6, are also used.

Channeling is reduced but does not disappear in polycrystalline materials [15]. The bigger the grain size, the more distinct the channeling effects are. Because of indirect or "scatter-in" channeling, where an ion which is not channelled at the surface of the target enters a channel as a result of random interatomic collisions, channeling is present in all low energy implants in crystalline and polycrystalline materials [10].

## 4 EXPERIMENTAL TECHNIQUES FOR MEASURING STOPPING AND RANGES

### 4.1 ELECTRONIC STOPPING

As experimental measurements of stopping powers are essential in determining the accuracy of electronic stopping parametrizations, a short review of the measurement techniques is in order. The methods currently in use for measuring electronic stopping can be divided into three categories [23]. In transmission methods the ion beam is allowed

to pass through a thin target and its energy is measured in front of and behind the target. In methods based on scattering or nuclear reactions the stopping powers are determined from the scattering or reaction yields. The third category consists of methods where the stopping powers are determined by first measuring the range distribution of implanted ions. The choice of method depends on the ion and the target material, the energy range examined and the equipment at hand.

Transmission methods are conceptually very simple: the energy of a low-intensity beam is measured before and after the target. One does not even need an accelerator, the stopping of e.g.  $\alpha$ -particles can be measured with a radioactive source. The target is usually a thin self-supporting foil, but stopping in gases, liquids and vapors can also be measured by placing the target between thin membranes (for gases, a differential pumped target can also be used). We can thus measure the stopping of any ion in any target. The energy resolution of the method is limited by the thickness of the target. This method cannot be used to measure stopping at very low energies, because the ions would deposit too much of their energy, or even stop, in the target. On the other hand, the properties of very thin films can be different from the properties of bulk materials [24]. Other problems with targets include pinholes and variations in thickness and composition. Furthermore, one must measure either the thickness or the surface density of the film. One technique is to weigh the film and measure its area by optical methods thus giving the surface density, another one is to determine the thickness by the transmission of  $\alpha$ -particles, profilometry or ellipsometry. Transmission methods can be used to measure the stopping of channeled ions [25].

Methods based on reactions or scattering determine the stopping from the yields of reactions or scatterings. An example of these methods is the inverted DSA (Doppler Shift Attenuation) method, where the stopping of a  $\gamma$  active ion is deduced from the lineshape of the  $\gamma$ -spectrum [26]. Obtaining accurate absolute stopping powers with these methods can be difficult because it often requires detailed knowledge on cross sections, measurement geometry, detector efficiency and ion current. This problem can be solved by measuring the stoppings relative to some known stopping. Methods based on reactions or scattering are usually not suitable for low velocities ( $v < v_0$ ).

In the third group of methods range distributions are measured by e.g. elastic recoil detection and the stopping is deduced from them. The implantation energy is varied and the changes in the range distribution are measured [29,I]. Except for secondary ion mass spectrometry, all ion beam analysis methods use stopping to fix the depth scale and therefore the stopping of the probing beam needs to be known. However, the energy of the probing beam is usually so high that its stopping is relatively easy to determine. These methods are useful in determining low velocity stopping powers which are difficult to determine by transmission methods. Moreover, range data is often useful in its own right. If the ion energies are very low, the surface roughness or surface impurities, e.g. an oxide layer, can affect the results. At high energies, on the other hand, the ions can go so deep into the target that the range profiles are difficult to measure. These methods can be

used to measure the stopping of practically any ion in any target. They can also be used to measure the stopping in channels.

## 4.2 RANGES

A short description of the methods utilized in measuring the range distributions used in this thesis, namely ERDA (Elastic Recoil Detection Analysis), NRB (Nuclear Resonance Broadening) and SIMS (Secondary Ion Mass Spectroscopy) is given below. In principle all of these methods can distinguish between different isotopes, although in practice ERDA cannot always separate the signals from different isotopes. In ERDA the energy of the detected particles tells us the depth and their number the concentration of the element we are measuring. In NRB, the depth scale is calculated from the slowing down of the probing ion beam. In both of these methods the depth resolution depends on the electronic stopping of the probing beam and we thus need to know it accurately. In SIMS, the depth information is deduced from the sputtering yields and time of detection. The depth resolution of all the aforementioned methods is better near the surface than deep inside the target. ERDA and NRB are practically nondestructive while SIMS destroys the part of the sample being measured. Typical uncertainties of depth scales are  $\pm 5\%$  for SIMS and  $\pm 10\%$  for NRB and ERDA, although the accuracy of the latter methods can be improved considerably by measuring the stopping of the probing beam accurately.

In NRB, a resonant nuclear reaction is utilized - that is, a reaction that will only take place if the energies of the nuclei are extremely close to a certain value (the resonance). An example of such a reaction is  ${}^1\text{H}({}^{15}\text{N}, \alpha\gamma){}^{12}\text{C}$ , which can be used to measure hydrogen concentrations with a nitrogen beam or vice versa. An ion beam whose energy is above the resonance energy is used; as the ions slow down in the target they reach the resonance energy and we get the concentration at that depth by measuring the gamma ray yield. This means that we have to perform one measurement for each point in the range distribution, which makes NRB a relatively slow technique. We also need a narrow resonance with a large cross section, which limits the range of isotopes that can be measured. On the other hand, NRB can be a very sensitive method with a detection limit as low as 10 parts per million (ppm) [27]. For a detailed discussion of the method, see e.g. Ref. [28]. The method is sometimes also called RNRA (Resonant Nuclear Reaction Analysis).

Elastic recoil detection analysis (ERDA) means that target atoms scattered in forward directions are detected. Signals from different elements have to be separated somehow, commonly used methods are foils placed in front of the detector [29], time-of-flight telescopes [30, 31] (TOF-ERDA),  $\Delta E$ -E telescopes [32] and magnetic filters [33] ( $E \times B$  ERDA). We get the range profiles of all elements from a single measurement, but we need to know the stopping powers of the probing beam and all the profiled elements. We can measure the range profiles of any atoms in any target, but the signals from elements with masses close to each other cannot always be separated. The mass resolution depends on the measurement system and the probing beam. Because of the small incident angles used, ERDA is sensitive to the surface roughness of the target [34].

In SIMS atoms, ions and molecular fragments which are sputtered from the sample surface by a low energy ion beam are mass analyzed to obtain chemical identification of the atoms present in the surface layer. SIMS is an extremely sensitive method and has a typical detection limit of less than a ppm. Additionally, one does not need to know any stoppings to interpret the measurements. In SIMS, a beam consisting of e.g. low energy oxygen ions is directed in to the sample. The beam sputters atoms from the sample and slowly erodes the sample. The depth scale can be fixed by measuring the depth of the resulting crater with a profilometer and dividing the result by the measurement time. Because of its sensitivity, SIMS is widely used in analyzing semiconductor samples. However, the technique has its problems. During sputtering both positively and negatively charged ions are detached from the sample along with clusters and neutral atoms. Two elements may have the same total sputtering yields, but the yields of sputtered ions can differ by a factor of 1000 [35]. Uncertainties in ionization probabilities are the biggest source of error in SIMS, especially absolute concentrations are difficult to determine without a standard. Another problem is interface roughening: although the sputtered atoms come mainly from the two topmost atomic layers of the target [36], the ions of the sputtering beam enter much deeper into the target and cause mixing thus degrading the depth resolution [37]. A recent alternative to SIMS is SNMS (Secondary Neutral Mass Spectrometry) [38], where the neutral atoms sputtered from the sample are extracted, ionized by laser and then analyzed. The use of SNMS circumvents the uncertainties in ionization probabilities and the method will therefore probably gain users during the next few years.

Before SIMS measurements became popular in the early eighties, differential capacitance-voltage profiling (C-V profiling) was used extensively. C-V profiling is a technique for obtaining depth distributions of electrically active dopants [39]. When a metal probe is brought in contact with a semiconductor surface, a space-charged depletion region and therefore a capacitor is formed at the junction. By applying a small alternating current (ac) voltage, the voltage derivative of the contact capacitance can be measured with a lock-in amplifier. The amplitude of the derivative signal is a function of the carrier concentration, and the sign gives the type of carrier. The local contact C-V measurements on standard doping samples show a monotonic behaviour of capacitance derivative ( $dC/dV$ ) versus doping concentration in the range of  $10^{14}$  to  $10^{18}$   $\text{cm}^{-3}$ . The differential capacitance method can be used to measure 2D distributions of electrically active dopants by repeating the measurement in different places on the sample surface. C-V profiling is widely used but profiles obtained from these measurements cannot be compared directly with distributions from range calculations.

Computer simulations yield not only one-dimensional depth profiles but also the three-dimensional distribution of dopants in the target. There have also been some attempts to measure three-dimensional range distributions. Two noteworthy approaches are the 3D atom probe and the modified tomographic reconstruction (MOTOR) technique of Mueller *et al.* [40].

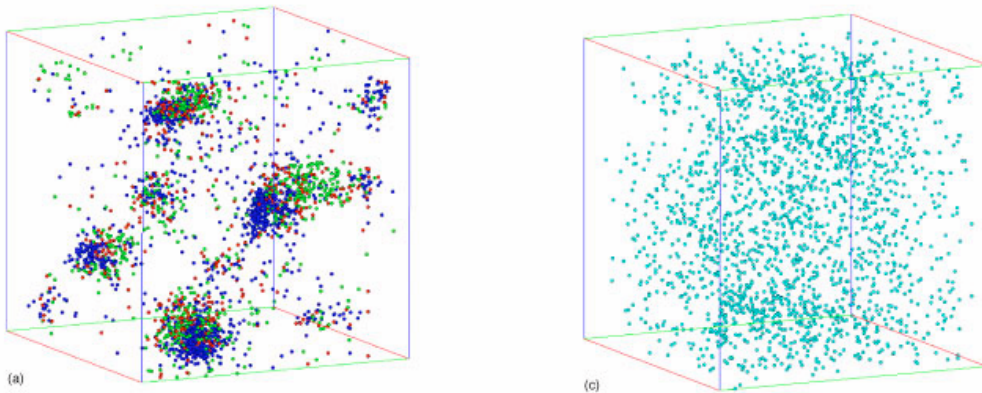


Figure 7: Three-dimensional element distributions from the analysis of Sandvik 1RK91 steel [41]. On the left, the blue dots represent Cu atoms and the green ones Ti atoms. On the right, the dots represent Mo atoms. The analysis volume is  $6 \text{ nm} \times 6 \text{ nm} \times 14 \text{ nm}$ .

A 3D atom probe is a combination of a field ion microscope (FIM) and a time-of-flight telescope [41]. The sample is sharpened to a tip with a very small radius. An electric field is applied between the sample and a position-sensitive target detector. A sufficiently high electric field detaches ions from the sample. These ions are attracted by the position-sensitive detector, their time of flight and point of impact are recorded [42, 43]. A spatial resolution of 0.3 nm can be achieved. The sensitivity of this technique is very good, comparable to SIMS. It has been used e.g. to study the three-dimensional structure of magnetic multilayer systems under consideration for memory applications [44]. If the mass resolution is maximized we can distinguish between different isotopes but experience a drop in the spatial resolution [41]. An example of a three-dimensional distribution measured by a 3D atom probe is shown in Fig. 7.

In the MOTOR technique developed by Mueller *et al.*, the three-dimensional distribution is reconstructed by performing several implants with different tilt angles and measuring a one-dimensional range profile from each. This technique works for samples that are amorphous or polycrystalline with a small grain size but can also be used for crystalline samples with relatively complicated target preparation [40]. The MOTOR technique is seldom used but is included here for completeness.

## 5 PRINCIPLES OF RANGE CALCULATIONS

The objective of range calculations is to calculate the distribution of dopants in the target materials. The results are presented as a one-dimensional or multidimensional distribution.



The computationally least demanding way of doing range calculations is to use analytical methods based on the Boltzmann transport equation [2, 13, 45–47]. They are not atomistic but rather treat the target as a continuous medium. Programs based on analytical models can calculate the moments of a range distribution in a matter of minutes, but the physics in these models is not very advanced and the accuracy of the results is not very good unless the model parameters can be adjusted on the basis of data from experiments or more detailed computer simulations. They can cope with multilayered structures [48] but cannot handle phenomena caused by the crystal structure, such as channeling. 2D profiles can be calculated but in this case the method slows down [49] (it is still faster than performing atomistic simulations). Analytical methods have been losing ground steadily as simulation models incorporating more physics have become computationally feasible, but they are still used in some cases [6], mainly because of their speed and ease-of-use. Computer programs which calculate ranges by solving the Boltzmann equation include PRAL [13] and the SUPREM [10] package.

Atomistic simulation programs can be divided into Molecular Dynamics (MD) and Binary Collision Approximation / Monte Carlo (BCA/MC) programs. They both calculate the time evolution of a system of atoms by solving its equations of motion numerically [46]. A range profile is constructed from many, usually 5000 - 50000, ion trajectories. Both atomistic methods yield the whole three-dimensional range distribution.

MD and BCA differ in the way they treat the nuclear stopping. BCA programs, such as TRIM [13], COSIPO [50] and MARLOWE [51], treat all interactions between atoms as binary collisions and calculate the trajectory one collision at a time, whereas in the MD method the atoms interact simultaneously with all their neighbours. The BCA programs either assume the target to be amorphous (TRIM) or take the crystal structure into account (COSIPO, MARLOWE, CTRIM). The latter type of programs are sometimes referred to as lattice-BCA programs. The binary collision approximation works well at high energies, but breaks down at low energies. As all ions eventually slow down and stop, they always leave the BCA realm of validity. If one wants to calculate accurate range profiles and the energy of the ions is less than about 1 keV/amu, MD methods should be used. Lattice-BCA programs can be used to calculate ranges under channeling conditions [52], but they contain parameters, such as the multiple collision parameter [51], that can have a considerable effect on the simulation results but have no clear physical meaning and whose values cannot be deduced from experiments [4]. In BCA simulations the effects of nuclear and electronic stopping can be difficult to separate, that is, an inaccurate electronic stopping model can be compensated by an inaccurate interatomic potential or a choice of parameters to give a range distribution in a reasonable agreement with experiment [53].

Molecular dynamics simulations are the most accurate but also the most time-consuming type of range calculations. In MD, atomic collisions are treated realistically and the results are accurate also at low velocities. The effects of electronic and nuclear stopping are thus easy to separate, which makes MD the method of choice in e.g. determining the

electronic stopping by comparing experimental and simulated range profiles [29]. We also get realistic damage distributions. As computers have become more powerful, the popularity of MD methods over BCA has increased [13, 54]. There have also been some attempts to combine the speed of BCA with the accuracy of MD by using BCA at high energies and switching over to MD as the ions slow down [55].

The change in the positions of particles is calculated from the interaction forces between them. We calculate these forces by differentiating the interatomic potential. Unlike in BCA, not only pair potentials but also many-body potentials can be used. In practice pair potentials can be used in range calculations, because the shape of the potential well is not very important in high-energy interactions [56]. The equations of motion, the form of which depends on the ensemble being simulated [5, 57], are solved numerically. Then the positions and velocities of the atoms are updated and we have completed one time step.

The accuracy of the simulation results depends on the quality of the interatomic potential. The potential is conventionally divided into repulsive and attractive parts, of which the repulsive part is the important one for range calculations. The repulsive part can be described as a screened Coulomb interaction,

$$V(r) = \frac{Z_1 Z_2 e^2}{r} \phi(r), \quad (4)$$

where the screening function  $\phi$  goes from one to zero as the distance between the nuclei increases. A large number of potentials, some semi-empirical, some theoretical, have been proposed over the years. A popular repulsive potential is the ZBL potential given by Ziegler, Biersack and Littmark [13]. The universal ZBL potential has been constructed by fitting a universal screening function to a large set of theoretically obtained pair potentials and can be off by ten percent [13]. To guarantee reliable results a more accurate potential has to be used. One way to obtain such potentials is to use self-consistent total energy calculations and the local density approximation (LDA) for electronic exchange and correlation energies [58]. In this approach the total energy is obtained as a function of the distance between the atoms in a dimer. The potentials used in the simulations for this thesis were calculated with this approach using the DMol density-functional package [59–61]. They are very accurate; in the study by Nordlund *et al.* [62] it was found that the difference between potentials calculated with DMol and those obtained by highly accurate [63] fully numerical Hartree-Fock-Slater calculations was at most 1%.

The simulations for this thesis were performed using programs based on MDRANGE [56, 64, 65]. It uses a version of the Smith-Harrison algorithm [66], which is a predictor-collector algorithm [67] allowing a variable time step, to solve the equations of motion. MDRANGE is an efficient MD program which uses several approximations to speed up the simulation and reduce the amount of memory needed. The five most important ones are listed below.

1. **Only a small part of the target lattice is simulated at a time.**

15 Å is a typical length of the simulation cell (the cell length should be a multiple of the

side of the crystal unit cell). When the ion approaches the edge of the cell, a new slice of the lattice is created in front of it.

**2. Only the interactions relevant to the ion are solved (RIA, Recoil Interaction Approximation).**

The target atoms do not experience any interactions they are not near the ion. RIA allows us to use repulsive potentials and forget about the attractive part of the potential.

**3. We use a special system of units to minimize the number of multiplications** in which e.g. all the masses  $\equiv 1$ .

**4. Atoms only interact with atoms that are close to them.**

3 Å is a typical cut-off radius, the neighbours are listed in a table which is updated when necessary.

**5. An algorithm that allows the use of a variable timestep is used**

so that we can use a short time step for fast ions and a longer one for slower ions.

These features make simulations in the keV-regime feasible.

When a crystal lattice is subjected to ion bombardment, crystal damage begins to accumulate. The growth of damaged regions inhibits channeling and therefore the range profiles of high dose and low dose implants will have different shapes [10]. There have been some attempts to model damage accumulation in range calculations, some of which are outlined below. Almost all damage models can be used in both MD and BCA simulations.

The model of Kang *et al.* [68] simulates the ion-induced amorphization of the target by rotating the crystal structure by a random angle. This model accounts for the general onset of amorphization but relies on an empirical relation and does not provide information of point defects. Crandle and Mulvaney [69] have proposed a model which simulates the accumulation of damage by switching between crystalline and amorphous slices of target material. This model keeps track of point defects as they are formed, but relies on an empirical determination of the displacement energy and the critical energy density for amorphization. There are also models that simulate the formation of point defects explicitly. One such model has been developed by Klein *et al.* [70], which simulates the formation of point defects, their recombination and the effects these defects have on the ranges of subsequently implanted ions. The final location of all interstitials and vacancies is recorded for each collision cascade and if the distance between a vacancy and an interstitial at the end of the cascade is less than the capture radius (about 2.33 Å for Si [70]) they are considered to be annihilated. Recombination with damage from previous cascades is accounted for by a statistical algorithm. Surviving defects are weighted and summed to obtain a point defect distribution as a function of depth, which is then used to modify the structure of the crystal that subsequent ions travel through.

A typical depth profile in a crystalline material has a shape consisting of a near-surface peak followed by a tail where the concentration is several magnitudes below the peak concentration. Hence, if we wish to have good statistics at all depths we will have to simulate hundreds of atoms that stop near the peak for every one that stops in the tail.

This problem can be solved by employing a rare event algorithm [8,III]. In this technique, we define several splitting depths. Ion that passes a splitting depth is replaced by  $N$  virtual ions, the statistical weight of each being divided by  $N$  (each real ion has a statistical weight of 1) [7, 8]. A virtual ion that passes a splitting depth is divided into new virtual ions in a similar way. As a new slice of the crystal lattice with random thermal displacements is built in front of the ions, the trajectories of the virtual ions quickly diverge.  $N$  is a small integer, usually 2 or 3 [7, 8] - a large  $N$  means that many virtual ions stop in the tail but because many virtual ions share the beginning of their trajectories, there are strong correlations in the data. Several algorithms have been proposed for the selection of the splitting depths. Beardmore and Grønbech-Jensen [8] split ions at depths where the total number of ions (ignoring weighting) becomes half of the number of real ions implanted. Rare event algorithms can be used in both MD and BCA programs.

## 6 GENERALLY USED ELECTRONIC STOPPING PARAMETRIZATIONS

Thanks to the advance in computer performance and developments in simulation programs that have taken place during the last 25 years, nuclear stopping can now be handled accurately in computer simulations. For example, the range calculation methods used in our laboratory in the seventies consisted of Monte Carlo programs that did not take the crystal structure into account [71–73]. Lattice-BCA methods [50] were taken into use in the mid eighties and MD methods [74] in the early nineties. Unfortunately, quantum mechanics tells us that electrons have strong wave characteristics and cannot be localized. Therefore electrons, unlike nuclei, cannot be treated as point masses and an accurate description of electronic stopping is a much harder problem. Attempts to predict the electronic slowing down accurately in channels have achieved success only during the last couple of years.

As can be seen in Fig. 1, the electronic stopping has a maximum, which is usually located at approximately  $2 - 5 v_0$ . The velocity dependence is the result of two competing phenomena: on one hand, the charge state of an ion increases as its velocity increases, on the other hand, the larger the velocity, the shorter the interaction time [13]. At velocities beyond the maximum the electronic stopping can be predicted relatively accurately within the framework of the Bethe-Bloch model [75, 76]. Below and particularly near the maximum the predicting is much more difficult.

Electronic stopping parametrizations are either local (the stopping depends on the position in the crystal) or non-local (the stopping is the same everywhere in the crystal). Non-local parametrizations are calibrated to work in an ideal "random direction" and cannot be used if channeling is significant.

Brandt-Kitagawa (BK) theory [77, 78] forms the basis of many modern electronic stopping theories including the one developed in this thesis. The BK theory makes simplifying assumptions about e.g. the shape of the ions' electron clouds and does not directly

take into account the quantum mechanical stopping cross section between an ion and the target atom electrons. Therefore all stopping models based on the theory are more or less phenomenological in nature. In the BK theory the electronic stopping of a heavy ion is factorized into two components, the effective charge  $Z_{\text{eff}}$  and the electronic stopping of a proton  $S_p$ ,

$$S_e = Z_{\text{eff}}^2 S_p(\rho, v), \quad (5)$$

where  $\rho$  is the local electron density and  $v$  the velocity of the ion. Atomic units ( $e = \hbar / (2\pi) = a_b = m_e = v_0 = 1$ ) will be used throughout the chapter unless indicated otherwise.

If we examine the stopping of an ion in different materials, we find that the stopping is not a monotonous function of the atomic number of the target but shows oscillations ( $Z_2$  oscillations). Similarly, the oscillations observed for the stopping powers of different ions in the same material are called  $Z_1$  oscillations. The amplitudes of the  $Z_1$  oscillations are increased if the ions are channeled [3]. The  $Z_1$  oscillations are understood to be an ion size effect, diminishing in amplitude as the velocity of the ion increases. If we calculate the stopping of protons using the local charge density,  $Z_2$  oscillations should not be a problem. On the other hand, the BK theory does not take the shell structure of the ions' electron cloud into account and thus cannot describe  $Z_1$  oscillations.

According to the BK theory, the Fermi velocity of the target electrons is determined as

$$v_F = \frac{1}{\alpha r_s}, \quad (6)$$

where the one-electron radius  $r_s = (3 / (4\pi\rho))^{1/3}$  and  $\alpha = (4/(9\pi))^{1/3}$ . We can now calculate  $v_r$ , the velocity of the ion relative to the electrons [13, 79],

$$v_r = v \left( 1 + \frac{v_F^2}{5v^2} \right), \text{ if } v \geq v_F \quad (7)$$

$$v_r = \frac{3v_F}{4} \left( 1 + \frac{2v^2}{3v_F^2} - \frac{v^4}{15v_F^4} \right), \text{ if } v < v_F. \quad (8)$$

The BK theory assumes that electrons with orbital velocities less than  $v_r$  are stripped [13, 78]. The reduced relative velocity  $y_r$  is defined as

$$y_r = \frac{v_r}{Z_1^{2/3}}. \quad (9)$$

In the BK theory, the shell structure of the ion is neglected and a centrosymmetric charge density

$$\rho(r) = \frac{N}{4\pi\Lambda^2 r} e^{-r/\Lambda}, \quad (10)$$

where  $\Lambda$  is the screening length (describes how the electrons screen the nucleus) and  $N$  the number of electrons bound to the ion, is used instead. Now we can write down the

formula for the internal energy of the ion and solve it [13, 77] to obtain an expression for the screening length,

$$\Lambda = \frac{2(1-q)^{2/3}a}{Z_1^{2/3}(1-(1-q)/7)}, \quad (11)$$

where the constant  $a = 0.24005$  and the charge fraction  $q$  is defined as

$$q = \frac{Z_1 - N}{Z_1}. \quad (12)$$

Now we need to express the charge fraction  $q$  as a function of the reduced relative velocity  $y_r$ . Ziegler *et al.* [13] give an expression,

$$q = 1 - e^{-0.95(y_r - 0.07)}, \quad (13)$$

which is a fit to experimental data. They note, however, that it should only be used if  $y_r \geq 0.1$  as there is very little experimental data below this velocity [13]. The use of equation (13) is problematic. If  $y_r < 0.07$ , it will give negative  $q$  values, meaning that the ion will gain, not lose, electrons which is clearly nonphysical. Of the ions simulated in this thesis, this situation can arise with arsenic and indium at low charge densities and with phosphorus at extremely low charge densities, but not with boron. The value of charge density, where the ionization fraction goes negative decreases slightly with increasing velocity (for example, for 2 keV As this occurs at  $r_s \approx 1.06 \text{ \AA}$  and for 100 keV As at  $r_s \approx 1.125 \text{ \AA}$ ). The stopping power will still be positive because it is proportional to the square of the effective charge. We made some simulations using the expression for ionization fraction given by Azziz *et al.* [80],

$$q = 0.89y_r - 0.30y_r^2 \quad (14)$$

which is always positive in the velocity range of this thesis, but the difference in the results was negligible. An expression valid also for low velocities is still desirable, but all we have at the moment is equation (13).

The effective charge can now be expressed as

$$Z_{\text{eff}} = \gamma Z_1, \quad (15)$$

where

$$\gamma = q + C(1-q) \ln \left( 1 + \left( \frac{4\Lambda}{r_s} \right)^2 \right). \quad (16)$$

The first term in the fractional effective charge  $\gamma$  describes distant collisions, where the electrons see only the charge  $q$ , and the second part close collisions, where the electrons have penetrated the electron cloud of the ion. The constant  $C$  is about 0.5 and is weakly dependent on  $r_s$ . It has a larger value when  $r_s$  is large (when the electron density is small) [77, 81]. We did some test simulations with the exact expression for  $C$  and came to the

conclusion that this dependence is not significant in this context. We use the value  $C = 0.5$  for all cases, as is done in other stopping parameterizations based on the BK theory [4, 8, 11, 13, 70, 82].

Now we are capable of calculating the effective charge; we still need an equation for the stopping of protons. For velocities below  $v_F$ , nonlinear density-functional calculations by Puska *et al.* [83–86] give the stopping of a proton as

$$S_{\text{Ech}} = \frac{3v}{k_F r_s^3} \sum_{l=0}^{\infty} (l+1) \sin^2(\delta_l(E_F) - \delta_{l+1}(E_F)), \quad (17)$$

where  $\delta_l(E_F)$  is the phase shift for the scattering of an electron at the Fermi energy and  $k_f$  the Fermi momentum. A computationally less demanding way is to calculate the stopping of protons with linear response theory [87],

$$S_{\text{lin}} = \frac{2v}{3\pi} \left( \ln \left( 1 + \frac{\pi}{\alpha r_s} \right) - \frac{1}{1 + \alpha r_s / \pi} \right), \quad (18)$$

where the constant  $\alpha = (4 / (9 \pi))^{1/3}$ , and multiply it by a correction factor [4] to obtain the result of Puska *et al.*,

$$S_p = S_{\text{lin}} G(r_s) = S_{\text{Ech}}. \quad (19)$$

For the correction factor  $G$  we use the equation

$$G(r_s) = 1.00 + 0.717r_s - 0.125r_s^2 - 0.0124r_s^3 + 0.00212r_s^4. \quad (20)$$

When  $r_s \ll 1$ , the correction factor approaches 1 as the results obtained from the linear response theory and the nonlinear formalism converge [86]. The correction factor should be used only when  $r_s < 6$ . Equations (17) and (18) are valid when  $v \leq v_F$ . If one wants to simulate high-energy implantation, another expression for the stopping of a proton can be inserted in the model.

A brief review of the most important stopping models based on the BK theory is given below.

Ziegler, Biersack and Littmark [13] developed a nonlocal stopping model, the so-called ZBL stopping. The value of the Fermi velocity is a constant depending on the target material and can have an empirical correction factor. The ion screening lengths also have correction factors [53]. The stopping of protons is obtained from a fit of eight parameters that have different values each elemental target material. The ZBL stopping is still widely used, mainly because it is easy to calculate for any material and is included in the popular simulation program TRIM [13]. Because of the numerous free parameters it is reasonably accurate but because it is a nonlocal parametrization it cannot be used if channeling is significant. The accuracy of the ZBL stopping powers can be improved by using range measurements to determine a correction factor [I].

Azziz, Brannon and Srinivasan developed the ABS stopping. The ABS model uses equation (16) for the stopping of proton. The original ABS [80] model was a nonlocal

model and treated the Fermi velocity of the target as a free parameter. It was not a very successful nor a physically well-motivated theory and is mentioned here mainly because it inspired other, more successful models. Azziz *et al.* later developed a local electronic stopping model [88], which was not based on the BK theory and did not achieve popularity.

Klein, Park and Tasch [11, 70] authored a local stopping model. This model used the same expressions for the charge fraction and stopping of proton as the ABS model, but calculates the stopping from a spherically symmetric charge distribution [13]. The model was implemented into the MARLOWE [51] simulation program and achieved success in the simulation of boron implants but could not give accurate results for arsenic [7].

Finally, Beardmore, Grønbech-Jensen and coworkers developed in several stages [4, 8, 82] a local stopping model. The BGJ model uses equations (13) and (19) for the charge fraction and the stopping of protons, respectively. The stopping of protons is calculated from a spherically symmetric charge distribution [13] but the Fermi velocity of the target is treated as a free parameter, just like in the ABS model. This parameter has a different value for each ion-target combination [89] and is meant to take into account the  $Z_1$  dependence of the electronic stopping cross section. The BGJ model therefore combines features from the models of Azziz and Klein. The original model [4] was found wanting and a new version was developed. This model includes a version of the Firsov model [90, 91] to describe the loss of kinetic energy due to momentum transfer between the electrons of the ion and those of the target atoms. The BGJ model has achieved remarkable accuracy but contains a free parameter and is therefore unsatisfactory from the physical point of view.

Not all electronic stopping models are based on the BK theory. Other electronic stopping models in use include the LSS [47] (nonlocal), Robinson [46] (local) and the aforementioned Firsov [90] (local) models.

## **7 RANGE CALCULATIONS AND STUDIES OF STOPPING POWERS**

### **7.1 CORRECTION FACTORS FOR THE ZBL STOPPING POWERS**

As outlined in chapter 5, the comparison of simulated and measured range distributions yields information on the electronic stopping. Because the interatomic potentials used in our MD simulations are very accurate [62], it is justified to assume that any differences between the simulated and experimental profiles are due to inaccuracies of the electronic stopping. In paper I, we used this method to determine experimental correction factors to the ZBL stopping. The range profiles of alpha particles in copper, chromium, molybdenum and nickel were simulated with our MD program and measured with ERDA. The targets had polycrystalline structures, so channeling was relatively unimportant and ZBL stopping could be used. By comparing the simulated and experimental profiles, we found



that in chromium and molybdenum the ZBL stopping had to be multiplied by a factor of 1.2 in order to reproduce the experimental results.

## 7.2 ION BEAM MIXING AND INTERATOMIC POTENTIALS

Ion beam mixing is one of the few experimentally measurable quantities that depend directly on the outcome of collision cascades. Mixing has been measured in a wide range of materials [92], but a direct comparison of simulations and experiments has not been achieved before because of the high beam energies used in most experiments. In paper II, we calculate ion beam mixing in silicon and compare the results with experiments done using metallic marker layers [92, 93].

The mixing is calculated using a scheme developed by Nordlund *et al.* [94], in which the primary recoil spectrum is calculated with an MD range program using repulsive pair potentials and the mixing caused by the primary recoils is calculated with full MD simulations employing many-body potentials. At primary recoil energies higher than 5 keV a cumulative method is used: we treat the primary as an incident ion and simulate its slowing down and the number of recoils created by it in the MD range program.

The mixing parameter  $Q$  is defined as

$$Q_{exp} = \frac{Dt}{\phi F_{D_n}}, \quad (21)$$

where  $D$  is an effective diffusion coefficient for mixing,  $t$  the implantation time,  $\phi$  the ion fluence and  $F_{D_n}$  the deposited nuclear energy per ion per unit depth.  $Q$  was calculated by using the equation

$$Q_{sim} = \frac{\int_0^{E_0} R^2(E)n(e)dE}{6n_0E_{D_n}}, \quad (22)$$

where  $E_0$  is the initial ion energy,  $E_{D_n}$  the nuclear energy deposited in the marker layer region,  $n_0$  the atomic density,  $R(E)$  the atomic relocation and  $n(E)dE$  the primary recoil spectrum.  $R^2(E)$  was fitted to all the  $\langle R^2 \rangle$  values obtained in Si by full MD and the cumulative method.

As can be seen from Table 1, the experimental and simulated results are in good agreement considering the large experimental uncertainties. Because most of the mixing is caused by the primary recoils we cannot say much about the properties of the Tersoff many-body potential. The measurements give, however, an experimental confirmation of the accuracy of the repulsive potentials used.

## 7.3 A LOCAL ELECTRONIC STOPPING MODEL BASED ON THE BK THEORY

We studied several stopping models including the BGJ model [4, 8, 82] and developed a local electronic stopping model based on the BK theory (papers III and IV). Our model

Table 1: Simulated ( $Q_{sim}$ ) and experimental ( $Q_{exp}$ ) mixing parameter values. The errors for the simulated values were obtained as follows. The fit for  $R^2(E)$  has an error of about 10%. The contribution of the recoil spectrum to the total error was estimated by using different spectra. These together lead to error of about 16%.

Ion (energy)	$Q_{sim}$ ( $\text{\AA}^5/\text{eV}$ )	$Q_{exp}$ ( $\text{\AA}^5/\text{eV}$ )
Ar (110 keV)	$33 \pm 5$	$25 \pm 9^a$
Ar (110 keV)	$36 \pm 5$	$58 \pm 32^b$
Kr (220 keV)	$45 \pm 7$	$34 \pm 6^a$
Ne (50 keV)	$22 \pm 3$	$40 \pm 13^a$
Xe (300 keV)	$52 \pm 8$	$44 \pm 7^a$

<sup>a</sup> Ref. [93]

<sup>b</sup> Ref. [95]

uses equations (13) and (19) for the charge fraction and the stopping of protons, respectively. We calculate both the effective charge and the stopping of proton from a three-dimensional charge distribution. The model has no free parameters and can be used to calculate the stopping of any ion in any target whose electron distribution can be acquired. We started by testing existing electronic stopping models. The model of Klein *et al.* was originally implemented into MARLOWE, a BCA program. It was reported to work well for boron implants but not for arsenic. Yang *et al.* [7] suggested that the reason for this might be that the electron cloud of boron is fairly centrosymmetric while that of arsenic is not. We implemented Klein's stopping model into an MD program. The simulated range profiles were too deep for both boron and arsenic. The simulated range profiles were too deep in the  $\langle 100 \rangle$  direction and much too deep in the  $\langle 110 \rangle$  direction. The agreement was no better for boron than for arsenic, suggesting that the explanation of Yang *et al.* is incorrect. The initial good agreement for boron in the  $\langle 100 \rangle$  direction is probably due to the limitations of MARLOWE. Beardmore *et al.* drew a similar conclusion in the case of the original BGJ model [4, 8].

The BGJ model was also tested and the accuracy of the new version incorporating a version of the Firsov model was found to be good. However, the BGJ model treats the Fermi velocity of the target material as a free parameter, which is adjusted for every ion-target combination. We decided to try to reach similar agreement without any free parameters.

The three-dimensional charge distribution of silicon was calculated using the Dawson-Stewart-Coppens formalism [96–99] and the Hartree-Fock wave functions calculated by Clementi and Roetti [100]. In this formalism, the charge density is given by

$$\rho_c(r) = \sum_{nl} \kappa_{nl}^3 \rho_{nl}(\kappa_{nl}r) + O\rho_3(r) + H\rho_4(r), \quad (23)$$

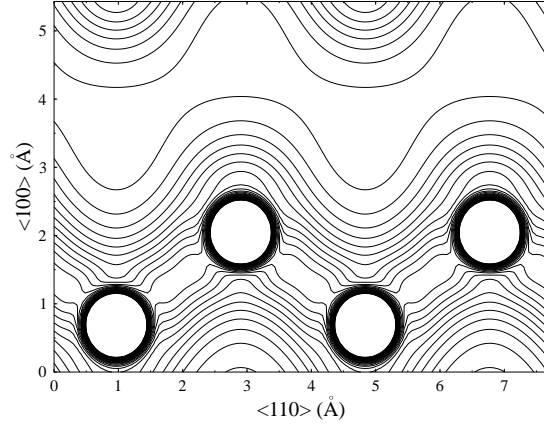


Figure 8: Calculated electron distribution of silicon in a (110) plane. The silicon atoms are clearly visible, as is the bond between the nearest neighbours. The contour interval is  $0.05 \text{ e} / \text{\AA}^3$  with contours going from 0.05 to 1.5 . The electron density is, of course, extremely high near the nuclei.

where  $n$  and  $l$  are quantum numbers defining the atomic orbital,  $\rho_{nl}$  the orbital charge densities,  $\kappa_{nl}$  the orbital expansion/contraction coefficients,  $\rho_3$  and  $\rho_4$  octopole and hexadecapole charge densities and  $O$  and  $H$  the octopole and hexadecapole electron populations [96, 101]. A cross section of the charge distribution can be seen in Fig. 8.

When the stopping of heavy ions is calculated, a version of the Firsov model is included to describe the energy loss due to electron transfer between the ion and target atoms. We use the approach derived by Elteckov *et al.* [102], where the slowing force (in Newtons) is given by

$$F(R, v) = \frac{-0.7h}{(\pi a_b)^2} \left( \frac{Z_A^2}{(1 + 0.8\alpha Z_A^{1/3} R/a_b)^4} + \frac{Z_B^2}{(1 + 0.8(1 - \alpha) Z_B^{1/3} R/a_b)^4} \right) v \text{ N}, \quad (24)$$

where  $R$  is the interatomic distance,  $a_b$  the Bohr radius ( $\approx 0.529 \text{ \AA}$ ),  $Z_A$  and  $Z_B$  ( $Z_A > Z_B$ ) the atomic numbers and  $\alpha = 1 / (1 + (Z_B/Z_A)^{1/6})$ . The validity of Firsov's original formulation [90, 103] is limited to cases where  $0.25 \leq Z_1/Z_2 \leq 4$  and although later formulations [91, 102] have tried to overcome this limitation, they still work best when  $Z_1 \approx Z_2$ . Therefore, the Firsov model is not used if the projectiles are protons. Some test simulations were performed, which confirmed that including the Firsov model would lead to a much too strong stopping.

The thermal displacements of lattice atoms have a strong effect on channeling [8]. The

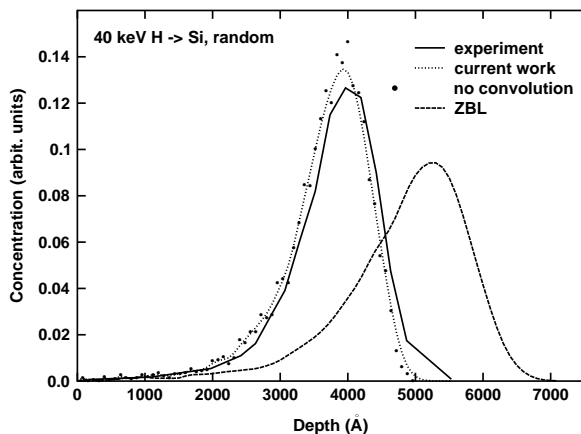


Figure 9: Simulated and measured ranges of 40 keV protons in silicon ( $\Theta = 8^\circ$ ,  $\phi = 0$ ). The reader should note that at these energies the velocity dependence of the stopping is not necessarily linear. The experimental profile was measured with NRB [27]. The electronic stopping accounts for approx. 99 % of the energy loss. The simulated profiles have been convoluted with the experimental resolution. A nonconvoluted simulated profile is shown as well to help the reader assess the importance of the convolution.

displacements are calculated from the Debye model and the Debye temperature is set such that the thermal displacements measured by Buschorn *et al.* [104] are reproduced.

Papers III and IV deal with different versions of our model. In paper IV, we test our electronic stopping model and compare it with other models. We first check the accuracy of the electronic stopping of protons and conclude that our model is a clear improvement over the ZBL also in non-channeling directions, see Fig. 8.

We then calculate range profiles of boron, arsenic, phosphorus and indium in silicon and compare the results with experimental profiles. All of the aforementioned are important dopants and are used extensively in the semiconductor industry [6, 105]. The results in non-channeling and  $\langle 100 \rangle$  directions are good, Figs. 10 and 11, those in  $\langle 110 \rangle$  are not very good. The agreement between the simulated and experimental profiles is generally slightly better at lower energies, which are also more interesting from the technological point of view. This is mostly due to the fact that the nuclear stopping, which the MD method takes into account very accurately, is more important there. Even at higher energies, where the electronic energy loss dominates, the agreement does not get significantly worse. Our equation for the stopping of protons assumes that the velocity of the ion is small compared to the Fermi velocity of the target electrons. This assumption, which

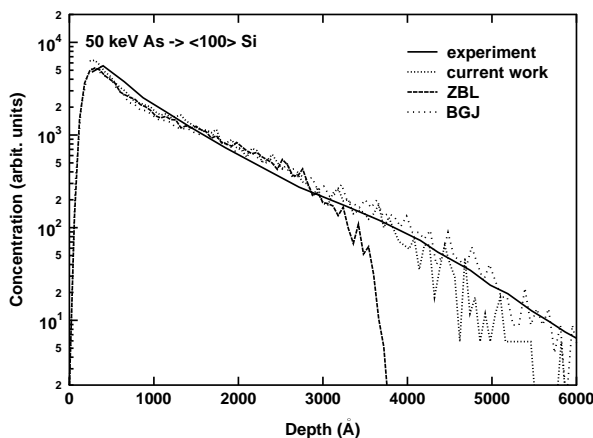


Figure 10: Simulated and measured ranges of 50 keV arsenic ions in the  $\langle 100 \rangle$  channel of silicon. The experimental range profiles were measured with SIMS [4]. The nuclear stopping accounts for approx. 68 % of the energy loss and the electronic stopping for 32 % (of which the Firsov model for 12 percentage points).

is inherent in all models using the model of Echenique and Puska for the stopping of protons [4, 8, 70, 82, 85], and the resulting velocity-proportional stopping both begin to break down at high energies (for example, the velocity of an 80 keV  $^{11}\text{B}$  is over  $0.5 v_0$ ). As can be seen in Fig. 12, using a three-dimensional charge distribution instead of a spherically symmetric one does improve the accuracy of the simulations.

In the  $\langle 110 \rangle$  direction we predict much longer tails than in the experimental profiles. We considered two possible reasons for this and concluded that the absence of thermal displacements in the electron distribution is not important at the simulation temperatures used. On the other hand, the use of the charge density at the center of the ion, instead of taking an average of the charge density experienced by the ion, does affect the results.

An averaging scheme was tested and it was found that as the averaging radius is increased,  $\langle 100 \rangle$  channels close first, followed by the  $\langle 110 \rangle$  channels. There is only a very small effect in non-channeling directions. This shows that much, if not most, of the remaining problems in the channels can be solved with an averaging scheme. However, to take  $Z_1$  oscillation properly into account a more realistic treatment of the electron cloud of the ion, instead of the exponential decay used in the BK theory and all stopping parametrizations based on it, is needed. This needs to be done because a satisfactory agreement for aluminum could not be achieved in any direction (this ion-target pair is known to present problems for other stopping models as well [89]). We hope that this matter can

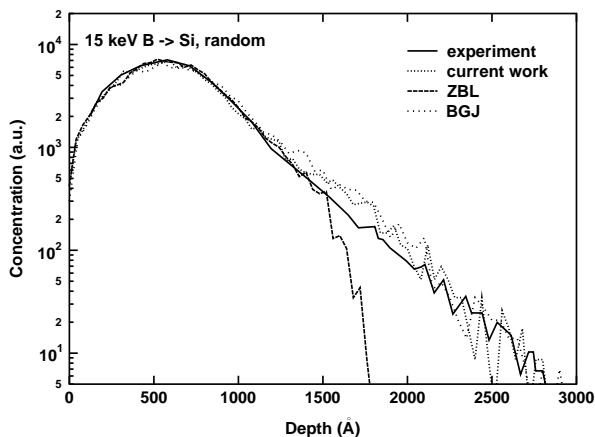


Figure 11: Simulated and measured ranges of 15 keV B ions in silicon ( $\Theta = 7^\circ$ ,  $\phi = 30^\circ$ ). The experimental range profile was measured with SIMS [8]. The nuclear stopping accounts for approx. 50 % of the energy loss and the electronic stopping for 50 % (of which the Firsov model for 22 percentage points).

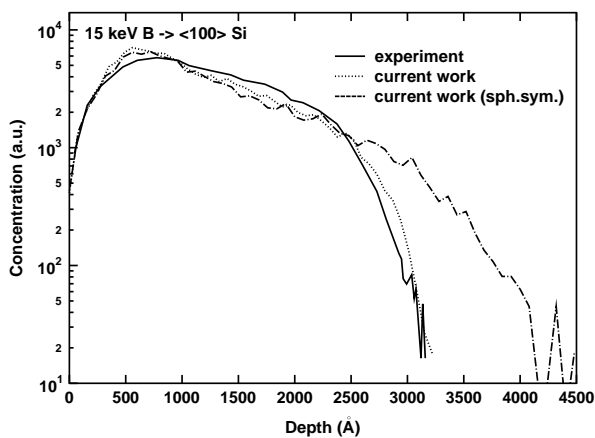


Figure 12: Effect of the charge distribution on the range profiles. The spherically symmetric distribution is from Ref. [13] and has been used in several electronic stopping models.

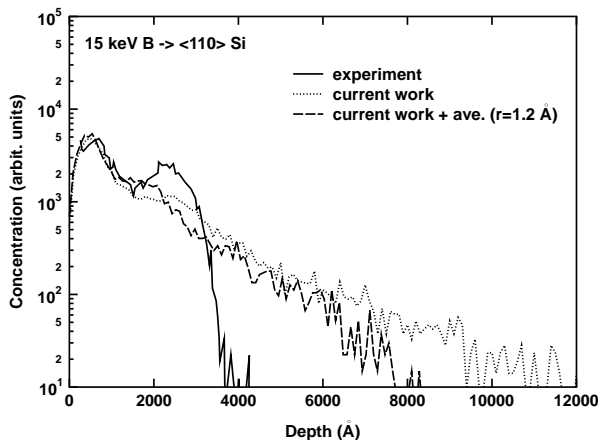


Figure 13: Effect of taking an average of the charge distribution when calculating heavy ion stopping. We took an average of the charge density inside a sphere of radius  $r = 1.2 \text{ \AA}$  and used it in the calculation of the effective charge. The results are not very sensitive to the value of the averaging radius.

be addressed in the near future.

## 8 CONCLUSIONS

We have studied the stopping of low-energy ions, electronic stopping in particular. We have, by using a method based on range measurements, determined the stopping of helium ions in several metals relevant to fusion research. We have also performed MD studies of ion-beam mixing and studied the possibility of using mixing experiments to develop better interatomic potentials.

The main body of this thesis deals with the problem of how to predict the electronic stopping of low-energy ions accurately in crystalline materials, a problem especially relevant to the semiconductor industry. We have tested several electronic stopping parametrizations and developed a model of our own. This model does not contain any free parameters, uses a three-dimensional electron distribution to describe the charge density of the target and thus represents a physically well-motivated approach. We have tested our model by calculating the ranges of several ions in silicon and comparing the results with experiments and simulations performed using other stopping models. The results obtained show that a three-dimensional electron distribution is a good basis for accurate, transferable stopping models.

## ACKNOWLEDGEMENTS

I wish to thank my supervisor, professor Juhani Keinonen, head of the Department of Physics, for his advice and guidance and for placing the facilities of the Department at my disposal. I also wish to thank the former and current heads of the Accelerator laboratory, Prof. Jyrki Räsänen and Dr. Eero Rauhala, for all the advice and support they have given me.

My sincere thanks are due to Prof. Kai Nordlund, whose tutoring, over the years, has been indispensable. All the co-authors and colleagues, who made taking this degree worthwhile, are also acknowledged, especially Dr. Ismo Koponen, Marcus Gustafsson, MSc, Dr. Kai Arstila and Jura Tarus, MSc.

Financial support from the Magnus Ehrnrooth Foundation and Vilho, Yrjö and Kalle Väisälä Foundation is gratefully acknowledged.

Helsinki, April 2000

*Jussi Sillanpää*



## References

1. *Handbook of modern ion beam analysis*, edited by J. Tesmer, M. Nastasi, J. Barbour, C. Maggiore, and J. Mayer (Materials Research Society, Pittsburgh, PA, USA, 1995).
2. *Ion beam modification of insulators*, edited by P. Mazzoldi and G. W. Arnold (Elsevier, Amsterdam, the Netherlands, 1987).
3. M. Nastasi, J. Mayer, and J. Hirvonen, *Ion-Solid Interactions - Fundamentals and Applications* (Cambridge University Press, Cambridge, Great Britain, 1996).
4. D. Cai, N. Grønbech-Jensen, C. M. Snell, and K. M. Beardmore, *Phenomenological electronic stopping-power model for molecular dynamics and Monte Carlo simulation of ion implantation into silicon*, Phys. Rev. B **54**, 17147 (1996).
5. J. von Boehm, *Molekyylidynamiikkamenetelmä* (Otatiето, Helsinki, 2000).
6. *The National Technology Roadmap For Semiconductors, 1998 update*, published by the Semiconductor Industry Association (SIA), 1998.
7. S. Yang, S. J. Morris, S. Tian, K. B. Parab, and A. F. Tasch, *Monte Carlo Simulation of Arsenic in (100) Single-Crystal Silicon*, IEEE Trans. Semiconductor Manufacturing 49 (1996).
8. K. M. Beardmore and N. Grønbech-Jensen, *An Efficient Molecular Dynamics Scheme for the Calculation of Dopant Profiles due to Ion Implantation*, Phys. Rev. E **57**, 7278 (1998).
9. Y. Taur, Y.-J. Mii, D. J. Frank, H.-S. Wong, D. A. Buchanan, S. J. Wind, S. A. Rishton, G. A. Sai-Halasz, and E. J. Nowak, *CMOS scaling into the 21st century: 0.1  $\mu\text{m}$  and beyond*, IBM J. RES. DEVELOP. **39**, 245 (1995).
10. *Handbook of ion implantation technology*, edited by J. F. Ziegler (North-Holland, Amsterdam, 1992).
11. K. M. Klein, C. Park, and A. F. Tasch, *Local electron concentration-dependent electronic stopping power model for Monte Carlo simulation of low-energy ion implantation in silicon*, Appl. Phys. Lett. **57**, 2701 (1990).
12. L. Montanet, K. Gieselmann, T. Associate, R. M. Barnett, D. E. Groom, T. G. Trippe, C. G. Wohl, B. Armstrong, G. S. Wagman, H. Murayama, J. Stone, J. J. H.

- F. C. Porter, R. J. Morrison, A. Manohar, M. Aguilar-Benitez, and C. Caso et al., *Review of particle properties*, Phys. Rev. D **50**, 1173 (1994).
13. J. F. Ziegler, J. P. Biersack, and U. Littmark, *The Stopping and Range of Ions in Matter* (Pergamon, New York, 1985).
  14. *Channeling*, edited by D. V. Morgan (John Wiley & Sons, New York, 1973).
  15. M. Hautala and R. Lappalainen, *Factors affecting the distributions of implanted ions*, Nucl. Instr. Meth. Phys. Res. B **28**, 519 (1987).
  16. M. T. Robinson and O. S. Oen, *Computer studies of the slowing down of energetic atoms in crystals*, Physical Review **132**, 2385 (1963).
  17. G. F. Piercy, F. Brown, J. A. Davies, and M. McCargo, *Experimental evidence for the increase of heavy ion ranges by channeling in crystalline structure*, Phys. Rev. Lett. **10**, 399 (1963).
  18. C. Park, K. Klein, A. Tasch, and J. Ziegler, *Critical Angles for Channeling of Boron Ions Implanted into Single-Crystal Silicon*, J. Electrochem. Soc. **138**, 2107 (1991).
  19. R. F. Lever and K. W. Brannon, *Crystallographic aspects of low energy boron implantation into silicon*, MRS Symp. Proc. **100**, 249 (1988).
  20. R. F. Lever and K. W. Brannon, *A low energy limit to boron channeling in silicon*, J. Appl. Phys **69**, 6369 (1991).
  21. D. V. Morgan and D. Van Vliet, *Computer studies of fast ion trajectories in crystals*, Can. J. Phys **46**, 503 (1968).
  22. D. Downey, C. Osburn, and S. Marcus, *Ultrashallow junction formation by ion implant and RTA*, Solid State Technology **Dec**, 71 (1997).
  23. K. Arstila, *Experimental Study of Electronic Stopping Powers for Heavy Ions*, Acta Polytechnica Scandinavica, Applied Physics Series **220**, 1 (1998), PhD thesis, University of Helsinki.
  24. P. Bauer, D. Semrad, and P. Mertens, *The Influence of Different Experimental Methods on the Measured Energy Dependence of Stopping Powers*, Nucl. Instrum. Meth. Phys. Res. B **12**, 56 (1985).
  25. A. Dygo, M. A. Boshart, M. W. Grant, and L. E. Seiberling, *Energy loss distributions for 625 keV  $H^+$  ions channeled near the  $\langle 100 \rangle$  axis in silicon*, Nucl. Instr. Meth. Phys. Res. B **93**, 117 (1994).

26. K. Arstila, J. Keinonen, and P. Tikkanen, *Stopping power for low velocity heavy ions*, Phys. Rev. B **41**, 6117 (1990).
27. P. Torri, J. Keinonen, and K. Nordlund, *A low-level detection system for hydrogen analysis with the reaction  ${}^1\text{H}({}^{15}\text{N}, \alpha\gamma){}^{12}\text{C}$* , Nucl. Instr. Meth. Phys. Res. B **84**, 105 (1994).
28. P. Torri, *Laitteisto pienten vetypitoisuuksien syvyysprofilointiin*, Master's thesis, University of Helsinki, 1992.
29. P. Haussalo, K. Nordlund, and J. Keinonen, *Stopping of 5 – 100 keV helium in tantalum, niobium, tungsten, and AISI 316L steel*, Nucl. Instr. Meth. Phys. Res. B **111**, 1 (1996).
30. J. Jokinen, J. Keinonen, P. Tikkanen, A. Kuronen, T. Ahlgren, and K. Nordlund, *Comparison of TOF-ERDA and nuclear resonance reaction techniques for range profile measurements of keV-energy implants*, Nucl. Instr. Meth. Phys. Res. B **119**, 533 (1996).
31. J. Jokinen, *Time-of-flight spectrometry of recoiled atoms in the analysis of thin films*, Acta Polytechnica Scandinavica, Applied Physics Series **212**, 1 (1997), PhD thesis, University of Helsinki.
32. J. P. Stoquert, G. Guillaume, M. Hage-Ali, J. J. Grob, C. Ganter, and P. Siffert, *Determination of concentration profiles by elastic recoil detection with a  $\Delta E$ -E gas telescope and high energy incident heavy ions*, Nucl. Instr. Meth. Phys. Res. B **44**, 184 (1989).
33. G. G. Ross and L. Leblanc, *Depth-profiling of hydrogen and helium isotopes by means of the ERD  $E \times B$  technique*, Nucl. Instr. Meth. Phys. Res. B **62**, 484 (1992).
34. T. Sajavaara, K. Arstila, A. Laakso, and J. Keinonen, *Effects of surface roughness on results in elastic recoil detection measurements*, Nucl. Instr. Meth. Phys. Res. B **161-163**, 235 (2000).
35. L. C. Feldman and J. W. Mayer, *Fundamentals of Surface and Thin Film Analysis* (North-Holland, Amsterdam, 1986).
36. H. Urbassek and H. M. Gades, *Molecular-dynamics simulation of adatom formation under keV-ion bombardment of Pt(111)*, Phys. Rev. B **50**, 11167 (1994).
37. J. Likonen, M. Hautala, and I. Koponen, *The effect of ion beam mixing on SIMS depth resolution*, Nucl. Instr. Meth. Phys. Res. B **64**, 149 (1992).

38. R. Jede, H. Peters, G. Duennebrier, O. Ganschow, U. Kaiser, and K. Seifert, *Quantitative depth profile and bulk analysis with high dynamic range by electron gas sputtered neutral mass spectrometry*, J. Vac. Sci. Technol. A **6**, 2271 (1988).
39. G. Dearnaley, J. H. Freeman, R. S. Nelson, and J. Stephen, *Ion Implantation* (North-Holland, Amsterdam, 1973).
40. D. Fink, M. Mueller, and L. Wang, *Reconstruction of three-dimensional range distributions by a modified tomographic technique*, J. Appl. Phys. **68**, 958 (1990).
41. A. Cerezo, T. J. Godfrey, S. J. Sijbrandij, G. D. W. Smith, and P. J. Warren, *Performance of an energy-compensated three-dimensional atom probe*, Rev. Sci. Instrum. **69**, 49 (1998).
42. B. Deconihout, C. Pareige, D. Blavette, and A. Menand, *Tomographic Atom Probe: New Dimension in Materials Analysis*, Microsc. Microanal. **5**, 39 (1999).
43. A. Cerezo, T. J. Godfrey, and G. D. W. Smith, *Application of a position-sensitive detector to atom probe microanalysis*, Rev. Sci. Instrum. **59**, 862 (1988).
44. D. J. Larson, A. K. Petford-Long, A. Cerezo, G. D. W. Smith, D. T. Foord, and T. C. Anthony, *Three-dimensional atom probe field-ion microscopy observation of Cu/Co multilayer film structures*, Appl. Phys. Lett. **73**, 1125 (1998).
45. *Ion Implantation Techniques*, edited by H. Ryssel and H. Glawischnig (Springer-Verlag, Berlin, 1982).
46. *Atomic & ion collisions in solids and at surfaces*, edited by R. Smith (Cambridge university press, Cambridge, UK, 1997).
47. J. Lindhard, M. Scharff, and H. E. Shiøtt, *Range concepts and heavy ion ranges*, Mat. Fys. Medd. Dan. Vid. Selsk. **33**, 1 (1963).
48. L. A. Christel, J. F. Gibbons, and S. Mylroie, *An Application of the Boltzmann Transport Equation to Ion Range and Damage Distribution in Multilayered Targets*, J. Appl. Phys. **51**, 6176 (1980).
49. M. D. Giles, *Ion Implantation Calculations in Two Dimensions Using the Boltzmann Transport Equation.*, IEEE Trans. Computer-Aided Design of Integrated Circuits and Systems **5**, 679 (1986).
50. M. Hautala, *Nuclear stopping in polycrystalline materials: range distributions and Doppler-shift attenuation analysis*, Phys. Rev. B **30**, 5010 (1984).

51. M. T. Robinson and I. M. Torrens, *Computer Simulation of atomic-displacement cascades in solids in the binary-collision approximation*, Phys. Rev. B **9**, 5008 (1974).
52. M. Hautala, *Channeling of B and As near the silicon (001) axis*, Nucl. Instr. Meth. Phys. Res. B **15**, 75 (1986).
53. R. J. Schreutelkamp, J. R. Liefting, P. M. Zagwijn, W. X. Lu, and F. W. Sarvis, *Addendum to Range straggling of MeV ions in amorphous silicon: discrepancies with TRIM*, Nucl. Instr. Meth. in Phys. Res. B **42**, 329 (1990).
54. T. Diaz de la Rubia, A. Caro, M. Spaczer, G. A. Janaway, M. W. Guinan, and M. Victoria, *Radiation-induced disordering and defect production in Cu<sub>3</sub>Au and Ni<sub>3</sub>Al studied by molecular dynamics simulation*, Nucl. Instr. Meth. Phys. Res. B **80/81**, 86 (1993).
55. M. Jaraiz, G. H. Gilmer, D. M. Stock, and T. Diaz de la Rubia, *Defects from implantation in silicon by linked Marlowe-molecular dynamics calculations*, Nucl. Instr. Meth. Phys. Res. B **102**, 180 (1995).
56. K. Nordlund, *Molecular dynamics simulation of ion ranges in the 1 – 100 keV energy range*, Comput. Mater. Sci. **3**, 448 (1995).
57. M. P. Allen and D. J. Tildesley, *Computer Simulation of Liquids* (Oxford University Press, Oxford, England, 1989).
58. W. M. C. Foulkes and R. Haydock, *Tight-binding models and density-functional theory*, Phys. Rev. B **39**, 12520 (1989).
59. R. O. Jones and O. Gunnarsson, *The density functional formalism, its applications and prospects*, Rev. Mod. Phys. **61**, 689 (1989).
60. J. Keinonen, A. Kuronen, K. Nordlund, R. M. Nieminen, and A. P. Seitsonen, *First-Principles Simulation of Collision Cascades in Si to Test Pair-Potential for Si-Si Interaction at 10 eV – 5 keV*, Nucl. Instr. Meth. Phys. Res. B **88**, 382 (1994).
61. J. Delley, *An all-electron numerical method for solving the local density functional for polyatomic molecules*, J. Chem. Phys. **92**, 508 (1990).
62. K. Nordlund, N. Runeberg, and D. Sundholm, *Repulsive interatomic potentials calculated using Hartree-Fock and density-functional theory methods*, Nucl. Instr. Meth. Phys. Res. B **132**, 45 (1997).

63. L. Laaksonen, P. Pyykkö, and D. Sundholm, *Fully numerical Hartree-Fock methods for molecules*, Computer Physics Reports **4**, 313 (1986).
64. K. Nordlund, *Molecular Dynamics Simulation of Atomic Collisions for Ion Irradiation Experiments*, Acta Polytechnica Scandinavica, Applied Physics Series **202**, 1 (1995), PhD thesis, University of Helsinki.
65. K. Nordlund and A. Kuronen, *Molecular dynamics simulation of ion ranges at keV energies*, Nucl. Instr. Meth. Phys. Res. B **115**, 528 (1996).
66. R. Smith and D. E. Harrison, Jr., *Algorithms for molecular dynamics simulations of keV particle bombardment*, Computers in Physics **Sep/Oct 1989**, 68 (1989).
67. D. Kahaner, C. Moler, and S. Nash, *Numerical methods and software* (Prentice Hall, Upper Saddle River, NJ, USA, 1989).
68. H. J. Kang, R. Shimizu, T. Saito, and H. Yamakawa, *Computer simulation of damage processes during ion implantation*, J. Appl. Phys **62**, 2733 (1987).
69. T. L. Cranley and B. J. Mulvaney, *An ion-implantation model incorporating damage calculations in crystalline targets*, IEEE Electron Device Lett. **11**, 42 (1990).
70. K. M. Klein, C. Park, and A. F. Tasch, *Monte Carlo Simulation of Boron Implantation into Single-Crystal Silicon*, IEEE Trans. Electron Devices **39**, 1614 (1992).
71. M. Luomajärvi, J. Keinonen, M. Bister, and A. Anttila, *Ranges of  $^{15}N^+$  ions in ten metals measured by  $(p, \alpha\gamma)$  resonance broadening*, Phys. Rev. B **18**, 4657 (1978).
72. J. Keinonen, M. Hautala, M. Luomajärvi, A. Anttila, and M. Bister, *Ranges of  $^{27}Al^+$  ions in nine metals measured by  $(p, \gamma)$  resonance broadening*, Radiation Effects **39**, 189 (1978).
73. A. Luukkainen, *Gammahuipun muodon laskeminen Monte Carlo -menetelmällä DSA-analyysissä*, Master's thesis, University of Helsinki, 1980.
74. A. Kuronen, *Molecular dynamics simulation of atom-atom collisional scattering*, J. Phys.: Condens. Matter **3**, 1363 (1991).
75. H. A. Bethe, *Zur Theorie des Durchgangs schneller Korpuskularstrahlen durch Materie*, Ann. Phys. **5**, 325 (1930).
76. F. Bloch, *Zur Bremsung rasch bewegter Teilchen beim Durchgang durch Materie*, Ann. Phys **16**, 285 (1933).

77. W. Brandt and M. Kitagawa, *Effective stopping-power charges of swift ions in condensed matter*, Phys. Rev. B **25**, 5631 (1982).
78. A. Mann and W. Brandt, *Material dependence of low-velocity stopping powers*, Phys. Rev. B **24**, 4999 (1981).
79. S. Kreussler, C. Varelas, and W. Brandt, *Target dependence of effective projectile charge in stopping powers*, Phys. Rev. B **23**, 82 (1981).
80. N. Azziz, K. W. Brannon, and G. R. Srinivasan, *Electronic stopping power for low energy ions*, MRS Symp. Proc. **45**, 71 (1985).
81. W. Brandt, *Modern problems of low-velocity stopping powers*, Nucl. Instrum. Methods **191**, 453 (1981).
82. D. Cai, C. M. Snell, K. M. Beardmore, and N. Grønbech-Jensen, *Simulation of phosphorus implantation into silicon with a single-parameter electronic stopping power model*, Int. J. Mod. Phys. C. **9**, 459 (1998).
83. M. Puska, *Theoretical studies of impurity-metal interactions*, Acta Polytechnica Scandinavica, Applied Physics Series **148**, 1 (1984), PhD thesis, Helsinki University of Technology.
84. M. J. Puska and R. M. Nieminen, *Atoms embedded in an electron gas: Phase shifts and cross sections*, Phys. Rev. B **27**, 6121 (1983).
85. P. M. Echenique, R. M. Nieminen, and R. H. Ritchie, *Density functional calculation of stopping power of an electron gas for slow ions*, Solid State Comm. **37**, 779 (1981).
86. P. M. Echenique, R. M. Nieminen, J. C. Ashley, and R. H. Ritchie, *Nonlinear stopping power of an electron gas for slow ions*, Phys. Rev. A **33**, 897 (1986).
87. R. H. Ritchie, *Interaction of Charged Particles with a Degenerate Fermi-Dirac Electron Gas*, Physical Review **114**, 644 (1959).
88. N. Azziz, K. W. Brannon, and G. R. Srinivasan, *Impact parameter dependent electronic energy losses*, Phys. Status. Solidi **b142**, 35 (1987).
89. K. M. Beardmore and N. Grønbech-Jensen, *An efficient molecular dynamics scheme for predicting dopant implant profiles in semiconductors*, Nucl. Inst. Meth. Phys. Res. B **153**, 391 (1999).

90. O. B. Firsov, *A qualitative interpretation of the mean electron excitation energy in atomic collisions*, Soviet Physics JETP **36(9)**, (1959).
91. L. Kishinevskii, *Cross sections for inelastic atomic collisions*, Bull. Acad. Sci. USSR, Phys. Ser. **26**, 1433 (1962).
92. B. M. Paine and R. S. Averback, *Ion beam mixing: basic experiments*, Nucl. Instr. Meth. Phys. Res. B **7/8**, 666 (1985).
93. S. Matteson, B. M. Paine, M. G. Grimaldi, G. Mezey, and M.-A. Nicolet, *Ion beam mixing in amorphous silicon I. Experimental investigation*, Nucl. Instr. Meth. Phys. Res. B **182/183**, 43 (1981).
94. K. Nordlund, L. Wei, Y. Zhong, and R. S. Averback, *Role of electron-phonon coupling on collision cascade development in Ni, Pd and Pt*, Phys. Rev. B (Rapid comm.) **57**, 13965 (1998).
95. B. M. Paine, M.-A. Nicolet, R. G. Newcombe, and D. A. Thompson, *Comparison of ion beam mixing at room temperature and 40K*, Nucl. Inst. and Meth. Phys. Res. **182/183**, 115 (1981).
96. M. Deutsch, *Electronic charge distribution in crystalline silicon*, Phys. Rev. B **45**, 646 (1992), **46** 607 (1992).
97. B. Dawson, *The covalent bond in silicon*, Proc. R. Soc. London, Ser A **298**, 379 (1967).
98. R. F. Stewart, *Electron population analysis with generalized X-ray scattering factors: higher multipoles*, J. Chem. Phys. **58**, 1668 (1973).
99. N. K. Hansen and P. Coppens, *Testing aspherical atom refinements on small-molecule data sets*, Acta Cryst. A **34**, 909 (1978).
100. E. Clementi and C. Roetti, *Roothaan-Hartree-Fock atomic wavefunctions*, Atomic Data and Nuclear Data Tables **14**, 177 (1974).
101. Z. W. Lu, A. Zunger, and M. Deutsch, *Electron charge distribution in crystalline germanium*, Phys. Rev. B **52**, 11904 (1995).
102. V. A. Elteckov, D. S. Karpuzov, Y. V. Martynenko, and V. E. Yurasova, in *Atomic Collision Phenomena in Solids*, edited by D. Palmer, M. W. Thompson, and P. D. Townsend (North-Holland, Amsterdam, 1970), Chap. ion penetration into Si single crystal, p. 657.



103. C. S. Murthy and G. R. Srinivasan, *Computer Simulation Studies of Ion Implantation in Crystalline Silicon*, IEEE Trans. Electron Devices **39**, 264 (1992).
104. G. Buschorn, E. Diedrich, W. Kufner, M. Rzepka, H. Genz, P. Hoffmann-Stascheck, and A. Richter, *Temperature dependence of planar channeling radiation in silicon, germanium, and beryllium between 12 and 330 K*, Phys. Rev. B **55**, 6196 (1997).
105. Y. Chen, B. J. Obradovic, M. Morris, G. Balamurugan, D. Li, A. F. Tasch, D. Kamenitsa, W. McCoy, S. Baumann, R. Bleier, D. Sieloff, D. Dyer, and P. Zeitzoff, *Monte Carlo simulation of heavy species (Indium and Germanium) implanted into Silicon*, J. Techn. Computer Aided Design (1999).